Journal of Materials Chemistry C

Competing Ferroelectric Polarization: Hydroxyl Flip-Flop versus Proton-Transfer Mechanisms

Journal:	*Journal of Materials Chemistry C*
Manuscript ID	TC-ART-01-2022-000233.R1
Article Type:	Paper
Date Submitted by the Author:	27-May-2022
Complete List of Authors:	Shimoi, Yukihiro; National Institute of Advanced Industrial Science and Technology, Research Center for Computational Design of Advanced Functional Materials (CD-FMat) Tsuzuki, Seiji; AIST Tsukuba Central 5, National Institute of Advanced Industrial Science and Technology (AIST) Kumai, Reiji; High Energy Accelerator Research Organization (KEK) , Institute of Materials Structure Science Sotome, Masato; The University of Tokyo Research Center for Advanced Science and Technology Horiuchi, Sachio; National Institute of Advanced Industrial Science and Technology (AIST), a. Electronics and Photonics Research Institute (ESPRIT)

ARTICLE

Competing Ferroelectric Polarization: Hydroxyl Flip-Flop versus Proton-Transfer Mechanisms

Received 00th January 20xx,
Accepted 00th January 20xx

DOI: 10.1039/x0xx00000x

Yukihiro Shimoi,[*a] Seiji Tsuzuki, ‡[a] Reiji Kumai, [b] Masato Sotome[c] and Sachio Horiuchi[*d]

Ferroelectricity above room temperature and a theoretical simulation of the spontaneous polarization are reported for a polar polymorph of 2,5-dihydroxybenzoic acid. The planar zigzag hydrogen-bonded chain of hydroxy groups geometrically permits two distinct mechanisms: flip-flop motion of hydroxy groups and concerted intermolecular proton transfer. Density functional theory calculations indicate that the polarizations of these two mechanisms are quite different in magnitude with the opposite sign. Both the experimental and theoretical investigations are consistently in favor of a flip-flop process: it is more favorable than proton-transfer in energy and quantitively explains the observed spontaneous polarization. Flip-flop type polarization reversal is also supported by the minimal effects of deuteration on the ferroelectric properties and stability.

Introduction

The field of ferroelectrics has just celebrated the centenary of the discovery of the Rochelle salt ($NaKC_4H_4O_6{\cdot}4H_2O$) crystal by Valasek in 1920.[1] To date, many studies have focused on the relationships between organic molecules and ferroelectricity and between hydrogen bonding and ferroelectricity. Extensive explorations of nontoxic lead-free ferroelectric alternatives for practical applications have resulted in the development of many dielectrics in which sequences of hydrogen-bonded polar molecules and/or ions offer switchable polarization. In organic molecular ferroelectrics, cooperative intermolecular proton transfer governs ferroelectric properties, as exemplified by croconic acid and imidazoles.[2,3] An exceptional case is that of the tricyclohexylmethanol crystal exhibiting the improper ferroelectricity with a tiny polarization (6×10^{-3} μC/cm^2).[4] Here, a "flip-flop" reorientation of the two hydroxy groups is found to switch the polarity of the hydrogen-bonded dimer. Whereas the two mechanisms have been mutually exclusive in these ferroelectrics owing to the hydrogen-bonded geometries, they may be regarded as competitive in some hydrogen-bonded compounds.[5,6] In the present paper, we achieved ferroelectricity above room-temperature in Form I crystals of 2,5-dihydroxybenzoic acid (DHBA) in which the infinite chains of ···OH···OH··· hydrogen-bonded molecules constitute a novel platform that geometrically permits these two distinct mechanisms. We compare the results from DHBA with those of another phenol crystal, 2-naphthol (NPTL), which also has an intermolecular hydrogen network [chemical structures are shown in Fig. 1 (a) and (b), respectively].

Modern theory of dielectric polarization[7-9] has improved our fundamental understanding of ferroelectrics, including organic ferroelectrics. Corresponding theoretical simulations of spontaneous polarization have been found to quantitively reproduce the experimentally optimized performance of many hydrogen-bonded organic ferroelectrics.[3] The spontaneous polarization vectors for the two mechanisms are simulated to be not only distinct in their magnitude but also opposite in direction to each other. Hence, neither can be uniquely defined unless the switching processes are specified. Let us recall that each polarization value is defined by the change in polarization between the nonpolar and polar structures. Because the two mechanisms are based on a common polar structure, their different polarizations come from distinct nonpolar structures, as detailed below.

Results and discussion

Commercially available DHBA is chemically stable and has been used as a novel matrix for laser desorption-ionization mass spectrometry.[10] There are two monoclinic polymorphs for DHBA.[11,12] Although their crystal structures are similar to each other, the DHBA Form II crystal[11] has the nonpolar space group $P2_1/n$ and cannot be ferroelectric owing to its antipolar molecular arrangement without any pseudosymmetries. By contrast, the Form I crystal[12] was extracted as a ferroelectric candidate from the Cambridge Crystal Structure Database (CSD) by searching for

[a] Research Center for Computational Design of Advanced Functional Materials (CD-FMat), National Institute of Advanced Industrial Science and Technology (AIST), AIST Tsukuba Central 2, 1-1-1 Umezono, Tsukuba, Ibaraki 305-8568, Japan. E-mail: y.shimoi@aist.go.jp
[b] Photon Factory, Institute of Materials Structure Science, High Energy Accelerator Research Organization (KEK), Tsukuba 305-0801, Japan.
[c] Research Center for Advanced Science and Technology, The University of Tokyo, 4-6-1 Komaba, Meguro-ku, Tokyo 153-8904, Japan.
[d] Research Institute for Advanced Electronics and Photonics (RIAEP), National Institute of Advanced Industrial Science and Technology (AIST), AIST Tsukuba Central 5, 1-1-1 Higashi, Tsukuba, Ibaraki 305-8565, Japan. E-mail: s-horiuchi@aist.go.jp

† Electronic Supplementary Information (ESI) available: Infrared absorption spectra, crystal data, theoretical spontaneous polarization, *P-E* hysteresis loops, calculated Born effective charge, and switching fields at various sweep rate. CCDC reference numbers 2088220 (DHBA), 2088221 (DHBA-d3) and 2088222 (NPTL). For ESI and crystallographic data in CIF or other electronic format see DOI: 10.1039/x0xx00000x.

‡ Current Addresses: Department of Applied Physics, The University of Tokyo, Tokyo, 113-8656, Japan.

polar crystals having a pseudo-inversion symmetry. Two datasets were available with a polar space group *Pa* (Ref codes: BESKAL01)[12] and nonpolar $P2_1/c$ symmetry (BESKAL02).[11] The pseudo-inversion symmetry in the former dataset is assumed in the latter analysis. This pseudosymmetry is located at the planar zigzag hydrogen-bonded chain of hydroxy groups at the C-5 position of DHBA and its emergence causes 1:1 positional disorder of the hydrogen atoms. We have also looked for other ferroelectric candidate phenols having similar hydrogen-bonded chains for a deeper understanding of the microscopic ferroelectric mechanisms of DHBA. The exploration of CSD led us to find a polar crystal structure of NPTL[13] with the monoclinic space group *Cc*, in which Marciniak et al. noted the presence of a pseudo-inversion for a centric *C*2/*c*-symmetry.[14] We re-examined the crystal structures of these two compounds as detailed in the following (Fig. 1).

A structural reassessment of Form I of DHBA was made on the electrically poled crystals to minimize the merohedral crystal twinning. The broken extinction rule for a few (0*k*0) reflections indicates a lowering of the crystal symmetry by loss of the inversion centers and the 2_1 screw axes. The revised crystal structure has the space group *Pc* (with the *a* and *c* axes interchanged from the dataset BESKAL01) and reproduced that previously reported, except that the hydroxy groups had fully ordered orientations. Table S1 includes the hydrogen-bonded O···O distance d_{OO}. Each carboxyl group participated in a cyclic hydrogen-bonded network to construct a molecular dimer (d_{OO} = 2.67–2.68 Å), and its carbonyl oxygen atoms also formed intramolecular hydrogen bonds with hydroxyl groups at the C-2 position with a slightly shorter d_{OO} (2.63–2.64 Å) (Fig. 1a). Conversely, the other hydroxyl groups at the C-5 position formed polar infinite chains of ···OH···OH··· hydrogen-bonds having a longer d_{OO} (2.73–2.77 Å) parallel to the crystal *a*-direction. Essentially the same crystal structure was determined for the deuterated DHBA-d_3 Form I crystal, except for a slight elongation of d_{OO} only in the cyclic hydrogen-bonds between carboxyl groups.

The polar infinite chains of ···OH···OH··· hydrogen-bonds were preferentially formed in monoalcohols and dialcohols by cooperative effects,[15] because a hydroxyl oxygen that donates its hydrogen in a hydrogen bond becomes a better hydrogen bond acceptor.[16,17] This hydroxyl oxygen atom is amphoteric, acting as both the hydrogen donor and acceptor. One of the most intriguing features is that the chain geometry can reverse its polarity not only by rotation (flip-flop) of hydroxyl groups but also through proton transfer (hopping/tunneling) motion over the hydrogen bonds as discussed in detail below.

In the only available dataset for NPTL (Ref code: NAPHOB03), the hydroxyl hydrogen is unusually positioned. Therefore, this reassessment amends its proper location over the hydrogen bond. The initial inspection suggests that the candidate space groups are *C*2/*c* and *Cc*. The choice of latter polar symmetry is justified by apparently more reliable results in refinement of parameters (see Table S1). The pseudosymmetry in NPTL appeared to be less pronounced, suggesting that the difference in reliability between the polar and nonpolar datasets is greater in NPTL than in DHBA: In the checkCIF procedure (Supporting

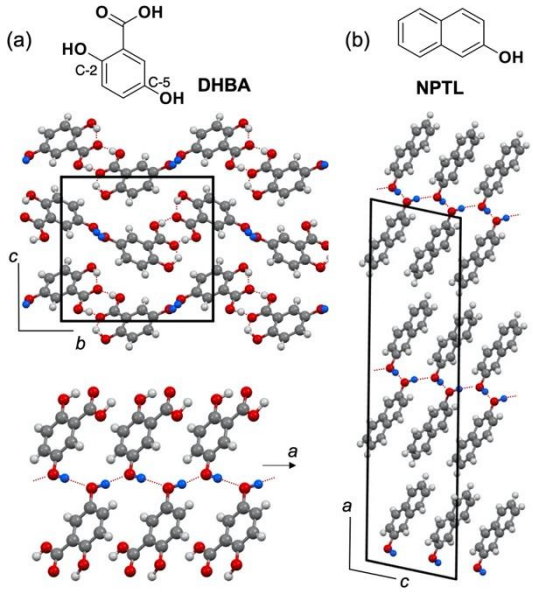

Fig. 1. Crystal structures and hydrogen bonding (red dotted lines). (a) (top) Projection of molecular arrangement in *a*-direction and (bottom) hydrogen-bonded polar chain viewed along *c*-direction for the DHBA Form I crystal. (b) Molecular arrangement of NPTL projected along *b*-direction.

Information) processed by the *PLATON* program,[18] the pseudosymmetry in the DHBA crystal is recognized at the alert level B, whereas noncrystallographic inversion is merely noted in NPTL at the alert level G. The NPTL has polar infinite chains of ···OH···OH··· hydrogen-bonds (d_{OO} = 2.74 Å similar to that of DHBA) parallel to the crystal *c*-direction (Fig. 1b).

The above-room-temperature ferroelectricity of a DHBA Form I crystal was confirmed from electric polarization versus electric field (*P*-*E*) hysteresis curves showing characteristic parallelograms (Fig. 2a). Note that the applied electric field is parallel to the polar infinite chains of ···OH···OH··· hydrogen-bonds in the crystal *a*-direction. The remanent polarization P_r is 4.4–5.2 μC/cm^2 and the coercive field E_c lies in the range of 20–60 kV/cm for a frequency range of 5–50 Hz. This polarization is moderately large among the single-component organic ferroelectrics showing the maximum of 30 μC/cm^2.[3,19]

The *P*-*E* measurements revealed that the high working temperature persists up to approximately 420 K, above which the ferroelectric hysteresis loops disappeared (Fig. 2b). Differential scanning calorimetry (DSC) measurements revealed corresponding anomalies with thermal hysteresis at 410–430 K (Fig. 2c). Note that this temperature is close to the highest Curie temperature observed among the single-component organic ferroelectrics (429 K for homochiral 10-camphorsulfonylimine).[20] The anomaly is split into two peaks, suggesting the presence of an intermediate phase with very narrow temperature interval above the first order phase transition. Note that the phase transitions were reversible and reproduced in the second run (Fig. S4a). This observation excludes the transformation to the crystal Form II, which did not show the corresponding phase

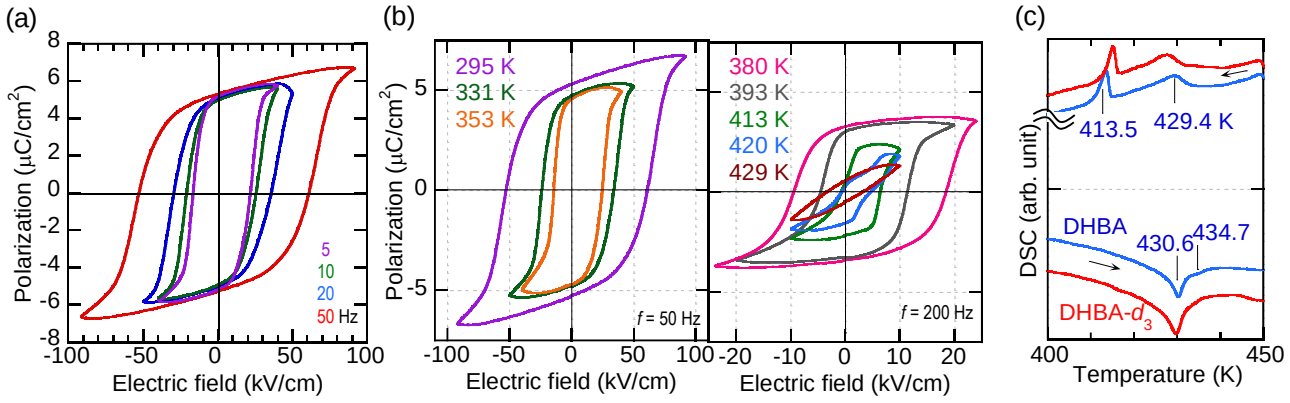

Fig. 2. Ferroelectric properties of DHBA Form I crystal at room temperature. (a) Electric polarization (P) versus electric field (E) hysteresis loops for a frequency range of 5–50 Hz. Applied electric field configuration of $\boldsymbol{E} \| \boldsymbol{a}$ is parallel to the hydrogen-bonded molecular chain. (b) Temperature dependence of P-E hysteresis loops. (c) Differential scanning calorimetry (DSC) thermographs of DHBA (blue) and deuterated DHBA-d_3 (red). Arrows indicate the directions of temperature changes at a rate of 5 K/min.

transitions in this temperature range. The observed total transition entropy of 0.68 J/K mol is much smaller than that ($\Delta S = R \ln g$ = 5.76 J/K mol, where R = 8.31 J/K mol) for the proton order-disorder phase transition mechanism having two possible configurations (g =2). Unfortunately, the thermal sublimation of specimens in air (Fig. S5) prevented us the attempts to obtain the changes of crystal structures, second harmonic generation (SHG), and permittivity at these phase transitions. Therefore, we could not definitely conclude whether the high-temperature phase is paraelectric or not.

The deuterated DHBA-d_3 Form I crystal had almost the same P_r (4.0 μC/cm²) (Fig. S6) and unchanged phase transition temperatures (Fig. 2c). However, the ferroelectricity of NPTL was not recorded as hysteresis loops even when a high field (as strong as 180 kV/cm) was applied along the crystal c-direction. This observation indicates that there is a larger energy barrier for ferroelectric switching in the NPTL crystal. Note that the DSC results of NPTL showed the absence of the paraelectric phase until the melting point (~390 K) (Fig. S4b).

The electric dipole moment in a finite system having charges q_i at positions $\boldsymbol{r}_i$ is defined by the total sum of $q_i\boldsymbol{r}_i$. In real periodic systems where electron wavefunctions extend over unit cells, such a classical treatment of polarization based on dipole moments breaks down and the Berry phase in quantum mechanics provides a valid theoretical description. On the basis of this approach, the spontaneous polarization is calculated along a path, which is defined by the parameter λ_i connecting the non-polar reference (paraelectric; λ_i = 0) state and the fully polarized (ferroelectric; λ_i = 1) state. Here, the suffix i = f and i = p represent the flip-flop (FF) and proton-transfer (PT) mechanisms, respectively. The experimentally observed spontaneous polarizations are uniquely defined as $\Delta P_i = P_i(1) - P_i(0)$ as far as the λ_i = 1 and λ_i = 0 states are specified on the same branch (the path i).

Here, we show that the PT and FF mechanisms provide distinct paths. Fig. 3 illustrates this situation schematically in the phenol crystals. Here, the structure at λ_i = 0 is the average of the λ_i = 1 structure and its inverted ferroelectric structure at λ_i = -1 except for the OH-hydrogen atoms. Each hydrogen atom is located at the center between a hydrogen-bonded O···O in the PT mechanism (the lower panel in Fig. 3). The atoms rotate around the hydroxyl C-O bond to give the inversion symmetry of the crystal in the FF mechanism (the upper panel in Fig. 3). More specifically, the position of the hydrogen at λ_p = 0 is unique in the PT mechanism; however, a degree of freedom remains in the FF mechanism because the inversion symmetry restricts only the relationship the rotation angle between symmetrically different hydroxy groups. In actual DFT calculations, we searched for the position giving the most stable energy within this constraint at λ_f = 0 for the FF mechanism in DHBA and NPTL. Considering the correlated proton dynamics suggested by the DSC results, we have employed the conventional procedure using the uniform model as the hypothetical paraelectric structure in the theoretical estimation of the polarization using the Berry phase.

The calculated polarizations of DHBA are nearly parallel to the a-direction: $\Delta\boldsymbol{P}_f(1)$ = (5.00, 0.00, -0.73) μC/cm² and $\Delta\boldsymbol{P}_p(1)$ = (-7.03, 0.00, -0.73) μC/cm² along the $\boldsymbol{a}$, $\boldsymbol{b}$, $\boldsymbol{c}^*$ crystal axes.

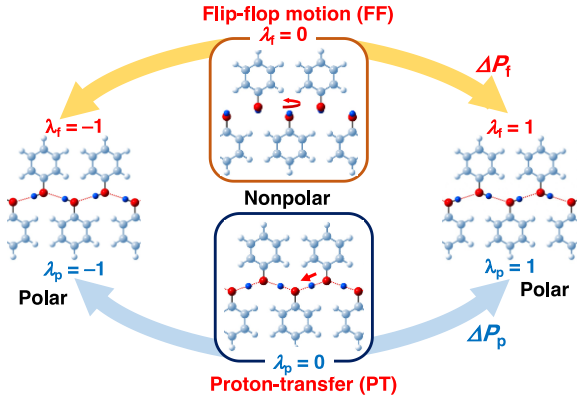

Fig. 3. Schematic illustration of PT and FF mechanisms during the polarization reversal. Arrows in red indicate the motional direction of hydrogen atoms from nonpolar (degree of distortion λ_i = 0) to fully polar state (λ_i = 1) (FF: i = f, PT: i =p), causing respective changes of polarization ΔP_p and ΔP_f.

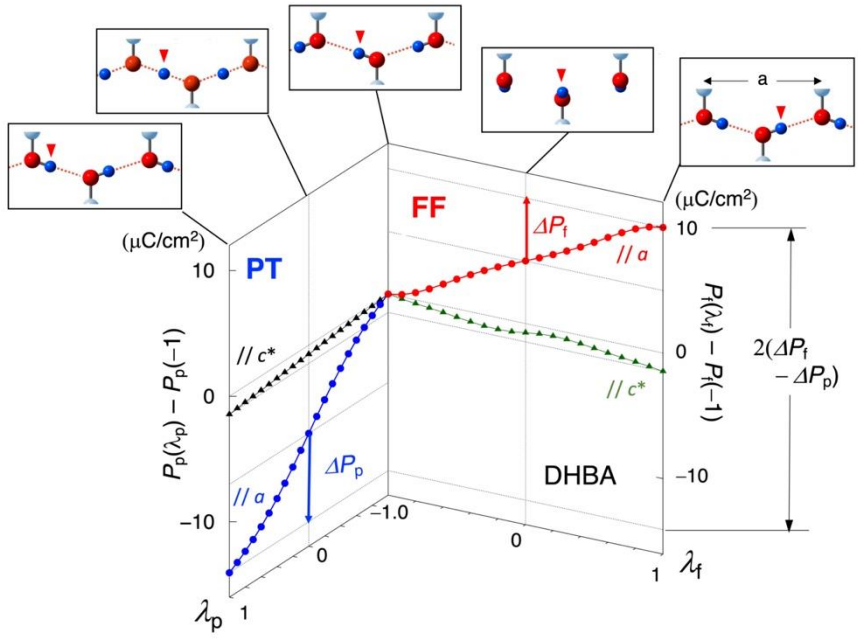

Fig. 4. The evolution of theoretical spontaneous polarization along the crystal *a* and *c** axes in DHBA Form I is plotted for the FF and PT mechanisms against the degree of polar distortion λ_i (FF: i = f, PT: i =p). λ_i = ±1 correspond to fully ferroelectric states with opposite directions in polarizations and λ_i = 0 is a centrosymmetric reference (hypothetical paraelectric state).

Comparison of these *a*-direction polarizations with the experimental P_r (5.2 μC/cm^2) is apparently in favor of the FF mechanism (with only 4 % difference) rather than PT (35 % difference). Figure 4 plots the evolution of calculated polarization from the λ_i = -1 state separately for the FF and PT mechanisms in DHBA. Note that polarization change on the pathway λ_f is positive and that on λ_p is negative. Despite the starting λ_f = -1 and λ_p = -1 structures being identical, the difference in polarization change along the crystal *a* axis reaches to $2(\Delta P_f - \Delta P_p)$ between the λ_f = 1 and λ_p = 1 structures after the complete polarization reversal. This difference is qualitatively understood by the fact that the pathways λ_f and λ_p are opposite in the direction of protons' displacement. The center of gravity of mobile hydrogen atoms, which is marked by the filled triangle in the schematic insets of Fig. 4, differs by the half of lattice constant $a/2$ between the λ_f = 1 and λ_p = 1 structures. To demonstrate this situation more explicitly and clarify the difference between the FF and PT processes, the positions of the protons are plotted as a function of λ_i in Fig. S7. Their displacements with increasing λ_i are opposite in direction between the two process as mentioned above. The difference between the FF and PT processes appears also in surface states as schematically illustrated in Fig. S8.

The *a*-direction component of $\Delta \boldsymbol{P}_f(1) - \Delta \boldsymbol{P}_p(1)$ = (12.02, 0.00, 0.00) μC/cm^2 perfectly agrees with the value of $e\boldsymbol{R}_a/\Omega$ = 12.01 μC/cm^2. Here, Ω = 6.62×10^{-22} cm^3 is the unit cell volume and $\boldsymbol{R}_a$ = 4.97×10^{-8} cm is the lattice constant along the crystal *a* direction with electronic charge *e*. The physical origin of polarization difference $2(\Delta P_f - \Delta P_p) = 2e\boldsymbol{R}_a/\Omega$ between the λ_f = 1 and λ_p = 1 structures is the shift of protons as (charge density) × (displacement) = $4e/\Omega \times a/2$ considering the unit cell accommodating 4 protons on 4 molecules. Note that as suggested by Born effective charge Z_{aa}* in Fig. S9 the protons have positive charges both in FF and PT and the mean value of the charge is estimated 1.06 (See the caption of Fig. S9). The similar argument can be made on NPTL (Ω = 1.51×10^{-21} cm^3; $\boldsymbol{R}_c$ = 8.12×10^{-8} cm (see Fig. S10): The value of $e\boldsymbol{R}_c/\Omega$ = 8.61 μC/cm^2 coincides $\Delta \boldsymbol{P}_f(1) - \Delta \boldsymbol{P}_p(1)$ = (-0.14, 0.00, 3.60) – (-0.14, 0.00, -5.01) = (0.00, 0.00, 8.61) μC/cm^2 along the ***a****, ***b***, ***c*** crystal axes.

Figure 5(a) and (b) show the energy profiles of the two mechanisms operating in DHBA and NPTL, respectively. The FF mechanism has a lower energy barrier for polarization reversal than that of PT for both compounds: The barrier heights of the FF mechanism were approximately 25% and 66% those of PT in DHBA and NPTL, respectively. This difference suggests that the former is more energetically favorable and is consistent with the observations in DHBA that the FF mechanism better explains the observed spontaneous polarizations than does PT. The FF process in the NPTL crystal requires a higher energy barrier than that in DHBA, which is also consistent with the experimental results that polarization does not reverse even with a stronger electric field in NPTL.

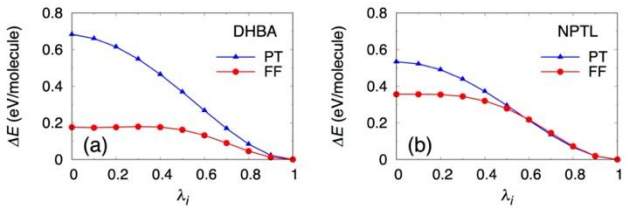

Fig. 5. Calculated energy profiles Δ*E* against the degree of polar distortion λ_i (FF: i = f, PT: i =p) in DHBA Form I (a) and NPTL (b).

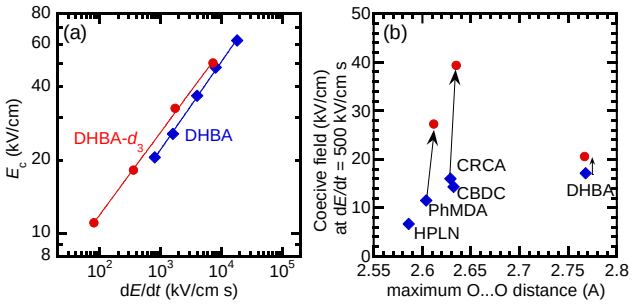

Fig. 6. Ferroelectric switching (coercive) field of DHBA and deuterated DHBA-d_3 crystals. (a) Variations with different field sweep rates dE/dt. (b) Switching field at dE/dt = 500 kV/cm s of DHBA and the OH···O bonded prototropic ferroelectrics: croconic acid (CRCA), 1-cyclobutene-1,2-dicarboxylic acid (CBDC), 2-phenylmalondialdehyde (PhMDA), and 3-hydroxyphenalenone (HPLN). Red filled circles with arrows indicate the changes of E_c for the deuterated specimens.

The electric field compels alignment of the total spontaneous polarization in the same direction. Therefore, the ideal way to uniquely identify the mechanism is to determine the OH hydrogen orientations with respect to the poling field. X-ray diffraction studies with MoKα (wavelength of 0.7108 Å) failed owing to the weak anomalous X-ray scattering effects[21] of light elements, C, H, and O in DHBA. Even at longer wavelengths (1.55 Å; ~8 keV) the differences of the Bijvoet pair (*hkl* versus *-h -k -l*) reflections were too small (less than 0.3%) for comparison, otherwise the peak intensity is insufficient (less than 1% of the most intense peak).

The effects of deuterium substitution on the hydrogen bonding provided an indirect indication about whether polarization reversal is based on the proton-transfer mechanism or not. Because deuterium has double the mass of a proton it has a much lower zero-point motion and a lower transfer probability than hydrogen. An extraordinarily large isotope effect should appear in the ferroelectric switching and the ferroelectric transition temperature. As a measure of the ease of switching, the switching (coercive) field of each *P-E* hysteresis loop was extracted at the peak field in the corresponding displacement current and the results are compared with those of typical proton-transfer type ferroelectrics.[2,3] The frequency-dependent *P-E* curves (e.g., Fig. 2a) show that the switching field E_c depends on the field sweep rate dE/dt. In Fig. 6a, the switching fields were systematically compared at a fixed sweep rate (0.5 MV/cm s). These values were obtained from a double logarithmic E_c – dE/dt plot through linear interpolation (See Fig. S11 for other prototropic ferroelectrics). As indicated by the arrows in Fig. 6b, the switching field is amplified on deuteration for prototropic ferroelectrics, such as croconic acid (CRAC) and phenylmalondialdehyde (PhMDA). In contrast, the switching fields were almost unchanged for deuteration of DHBA (Fig. 6a). Therefore, the ferroelectric mechanism of the DHBA crystal can be attributed to a FF process rather than PT. The same conclusion can also be argued on the basis of the relationship between the magnitudes of the switching field and the longest O···O separation of the corresponding hydrogen-bonds, as shown in Fig. 6b. Whereas the positive correlation observed among prototropic ferroelectrics[3] manifests as elongation of hydrogen bonds, which lifts the energetic barrier for PT processes, PT is an unlikely mechanism for DHBA crystals, because of the unexpectedly low switching field despite the O···O distances being approximately 0.14 Å longer than those of the prototropic ferroelectrics. On the other hand, with elongation of O···O distance, the weakened hydrogen bonds are more easily subject to their break and repair more easily, thus promoting the FF processes. Therefore, the shortening the hydrogen bonds with pressurization would interchange the preference between the FF and PT mechanisms.

Conclusions

We have demonstrated a new hydrogen-bonded ferroelectric molecular crystals of DHBA having a moderately large polarization of c.a. 5 μC/cm^2 and high working temperatures up to 420 K. The crystal structure was redetermined in this work and was consistent with its ferroelectric nature. The DHBA crystal is the first proper ferroelectric having the hydroxyl flip-flop mechanism, and also an exotic example permitting proton transfer geometrically as an additional competitive mechanism. The theoretical computation revealed that the changes of polarization between the fully polar structure and its symmetry-inverted one depend on these paths and differ from each other in both magnitudes and signs. The DFT calculations revealed that the barrier height of the flip-flop process was 25% lower than that of proton-transfer, the alternative plausible ferroelectric mechanism in DHBA. Flip-flop type ferroelectricity is supported by the quantitative agreement between the theoretical and experimental spontaneous polarization and can also consistently explain the least effects of deuteration on ferroelectricity.

Experimental sections

Sample preparation and characterization

Commercially available DHBA and NPTL were recrystallized twice from aqueous ethanol and chloroform, respectively. Colorless rod-shaped single crystals of DHBA Form I were grown by vacuum sublimation or slow evaporation of acetone solution at room temperature (Fig. S1a). The nonpolar Form II was crystallized as colorless (elongated) platelets from alcoholic or aqueous solutions. The two polymorphs[11] are often difficult to distinguish from their crystal appearance but are easily identified by their infrared spectra (Fig. S2b), and more conveniently by their cutting behavior; Form II specimens can be smoothly cleaved, whereas Form I crystals usually crack into pieces with rough edges. Reddish plates of NPTL were grown by temperature-gradient sublimation under reduced pressure and recrystallization (Fig. S1b). The deuterated DHBA-d_3 Form I crystals were obtained by sublimation under reduced pressure after recrystallization from deuterium oxide (99.9 %D) solution. The three hydroxyl groups were approximately 63% deuterated according to infrared vibrational spectra (Fig. S2a) measured on a KBr disk using a JASCO FT/IR-6600; the number of residual undeuterated species was estimated from the decrease of the O-H stretching band intensity at 2750–3550 cm^{-1} on the basis of the C=O stretch band intensity at 1640–1740 cm^{-1} as a relative standard. All attempts for obtaining further deuterium-enriched specimens were

unfortunately failed, because of the predominant crystallization of unwanted non-ferroelectric form II. Thermal analysis was performed using a differential scanning calorimeter (DSC7000X; Hitachi High-Technologies Corp., Tokyo). The sample was encapsulated in an aluminum pan and heated/cooled at 5 K/min. The temperature was calibrated to the melting point of indium (429.8 K).

Crystallographic studies

The crystal structure determination of the deuterated DHBA-d_3 Form I crystals and corresponding structural assessments of both the DHBA and NPTL crystals were performed in a four-circle diffractometer equipped with a hybrid pixel detector (Rigaku AFC10 with PILATUS200K; graphite-monochromated MoKα radiation). The ferroelectric DHBA crystal was poled through *P-E* hysteresis experiments prior to collection of the single crystal X-ray diffraction data. The intensity data were analyzed with the CrystalStructure crystallographic software packages (Molecular Structure Corp. and Rigaku Corp.). The final refinements were performed with anisotropic and isotropic atomic displacement parameters for the non-hydrogen atoms and the hydroxyl hydrogen atoms, respectively, and with a fixed C–H bond length of 0.95 Å for the hydrogen atoms. The crystallographic data and experimental details are summarized in Table S1.

Electrical measurements

All electric measurements were based on single crystals with painted silver paste electrodes. The *P–E* hysteresis curves were measured by a virtual ground method[22] using a ferroelectric substance evaluation system (Toyo Corporation, FCE-1), which comprised a current/charge–voltage converter (Toyo Corporation Model 6252), arbitrary waveform generator (Biomation 2414B), analogue-to-digital converter (WaveBook 516), and voltage amplifier (NF Corporation, HVA4321). All the crystals were immersed in silicone oil to avoid an electric discharge.

DFT calculations

Density functional theory (DFT) calculations were performed under periodic boundary condition using the generalized gradient approximation (GGA) functional of the Perdew–Burke–Ernzerhof (PBE) type[23] with the projector augmented-wave (PAW) method.[24] The cutoff energy was set to be 80 Ry for wave functions and 400 Ry for charge densities. The polarizations were calculated by the Berry phase.[7-9] The positions of non-hydrogen atoms were taken from the experimental data determined for the ferroelectric phases (λ_i = 1) of DHBA and NPTL and the hypothetical paraelectric phase (λ_i = 0) with *C*2/*c* symmetry of NPTL. Here, λ_i represents the parameters λ_f and λ_p connecting the non-polar and polar structures for the flip-flop (FF) and proton-transfer (PT) mechanisms, respectively. Those in the paraelectric phase of DHBA were obtained by the ADDSYM function in the *PLATON* software.[18] The positions of hydrogen atoms at λ_i = 0 and 1 were optimized with **k**-sampling of a 2 × 1 × 1 mesh for DHBA and 1 × 3 × 2 for NPTL. For intermediate structures between the para- and ferroelectric phases ($0 < \lambda_i < 1$), no further optimizations were performed, and the atomic positions were interpolated between the two phases: In the FF mechanism, the protons in the hydrogen-bonding chains at finite λ_f are expressed as a combination of rotations and translations and as translations for other atoms. All the DFT calculations were performed using the Quantum ESPRESSO package (version 6.5).[25,26] The validity of calculation procedures was confirmed by reproducing polarization values from previous works summarized in Ref 19 on some PT-type organic ferroelectrics (see Fig. S3).

Author contributions

Y. Shimoi and S. Horiuchi conceived the research ideas. S. Horiuchi is responsible for the preparation and electric measurements of the samples. Y. Shimoi and S. Tsuzuki contributed to the theoretical calculations. R. Kumai and M. Sotome contributed to the X-ray diffraction and nonlinear optical measurements, respectively. Y. Shimoi and S. Horiuchi wrote the manuscript. S. Horiuchi directed the project.

Conflicts of interest

There are no conflicts to declare.

Acknowledgements

SH thanks Fuminori Kamada for the IR spectroscopy measurements. This work was partially supported by JSPS KAKENHI Grant Number 21H04679 and JST CREST Grant Number JPMJCR18J2, Japan.

Notes and references

1 J. Valsek, Piezo-Electric and Allied Phenomena in Rochelle Salt, *Phys. Rev.*, 1921, **17**, 475-481.
2 S. Horiuchi, F. Kagawa, K. Hatahara, K. Kobayashi, R. Kumai, Y. Murakami, Y. Tokura, Above-room-temperature ferroelectricity and antiferroelectricity in benzimidazoles, *Nat. Commun.*, 2012, **3**, 1308.
3 S. Horiuchi, K. Kobayashi, R. Kumai, S. Ishibashi, Proton tautomerism for strong polarization switching, *Nat. Commun.*, 2017, **8**, 14426.
4 P. Szklarz, G. Bator, Pyroelectric properties of tricyclohexylmethanol (TCHM) single crystal, *J. Phys. Chem. Solids*, 2005, **66**, 121.
5 W. Saenger, C. Betzel, B. Hingerty, G. M. Brown, Flip-flop hydrogen bonding in a partially disordered system, *Nature*, 1982, **296**, 581-583.
6 P. Chen, M. Marianski, C. Baldauf, H-Bond Isomerization in Crystalline Cellulose III_I: Proton Hopping versus Hydroxyl Flip-Flop, *ACS Macro Lett*., 2016, **5**, 50-54.
7 R. D. King-Smith, D. Vanderbilt, Theory of polarization of crystalline solids, *Phys. Rev. B*, 1993, **47**, 1651-1654(R).
8 R. Resta, Macroscopic polarization in crystalline dielectrics: the geometric phase approach, *Rev. Mod. Phys.*, 1994, **66**, 899-916.
9 N. A. Spaldin, A beginner's guide to the modern theory of polarization, *J. Solid State Chem.*, 2012, **195**, 2–10.
10 K. Strupat, M. Karas, F. Hillenkamp, 2,5-Dihidroxybenzoic acid: a new matrix for laser desorption-ionization mass spectrometry, *Int. J. Mass Spectrom. Ion Processes*, 1991, **72**, 89–102.
11 D. E. Cohen, J. B. Benedict, B, Morlan, D. T. Chiu, B. Kahr, Dyeing Polymorphs: The MALDI Host 2,5-Dihydroxybenzoic Acid, *Cryst. Growth Des.*, 2007, **7**, 492-495.

12 M. Haisa, S. Kashino, S. -I. Hanada, K. Tanaka, S. Okazaki, M. Shibagaki, The structures of 2-hydroxy-5-methylbenzoic acid and dimorphs of 2,5-dihydroxybenzoic acid, *Acta Crystallogr. Sect. B*, 1982, **38**, 1480-1485.
13 H. C. Watson, A. Hargreaves, A. The crystal structure of β-naphthol, *Acta Crystallogr.*, 1958, **11**, 556.
14 B. Marciniak, E. Rozycka-Sokolowska, V. Pavlyuk, 2-Naphthalenol, *Acta Crystallogr. Sect. E*, 2003, **59**, o52-o53.
15 R. Taylor, C. F. Macrae, Rules governing the crystal packing of mono-and dialcohols, *Acta Crystallogr. Sect B*, 2001, **57**, 815-827.
16 J. Del Bene, J. A. Pople, J. A. Theory of Molecular Interactions. I. Molecular Orbital Studies of Water Polymers Using a Minimal Slater-Type Basis, *J. Chem. Phys*. 1970, **52**, 4858-4866.
17 C. Ceccarelli, G. A. Jeffrey, R. Taylor, A survey of O-H···O hydrogen bond geometries determined by neutron diffraction, *J. Mol. Struct.*, 1981, **70**, 255-271.
18 A. L. Spek, Single-crystal structure validation with the program *PLATON*, *J. Appl. Cryst*., 2003, **36**, 7-11.
19 S. Horiuchi, S. Ishibashi, Hydrogen-Bonded Small-Molecular Crystals Yielding Strong Ferroelectric and Antiferroelectric Polarizations, *J. Phys. Soc. Jpn.*, 2020**, 89**, 051009.
20 P.-F. Li, Y. Ai, Y.-L. Zeng, J.-C. Liu, Z.-K. Xu, Z.-X. Wang, Highest-T_c single-component homochiral organic ferroelectrics, *Chem. Sci.*, 2022, **13**, 657-664.
21 J. M. Bijvoet, A. F. Peerdeman, A. J. van Bommel, Determination of the Absolute Configuration of Optically Active Compounds by Means of X-Rays, *Nature*, 1951**, 168**, 271-272.
22 T. Schenk, E. Yurchuk, S. Mueller, U. Schroeder, S. Starschich, U. Böttger, T. Mikolajick, About the deformation of ferroelectric hysteresis, *Appl. Phys. Rev.*, 2014, **1**, 041103.
23 J. P. Perdew, K. Burke, M. Ernzerhof, Generalized Gradient Approximation Made Simple, *Phys. Rev. Lett.*, 1996, **77**, 3865-68.
24 P. E. Blöchl, Projector augmented-wave method, *Phys. Rev. B*, 1994, **50**, 17953-17979.
25 P. Giannozzi, S. Baroni, N. Bonini, M. Calandra, R. Car, C. Cavazzoni, D. Ceresoli, G. L. Chiarotti, M. Cococcioni, I. Dabo, A. Dal Corso, S. de Gironzoli, S. Fabris, G. Fratesi, R. Gebauer, U. Gerstmann, C. Gougoussis, A. Kokalj, M. Lazzeri, L. Martin-Samos, N. Marzari, F. Mauri, R. Mazzarello, S. Paolini, A. Pasquarello, L. Paulatto, C. Sbraccia, S. Scandolo, G. Sclauzero, A. P. Seitsonen, A. Smogunov P. Umari, R. M. Wentzcovitch, QUANTUM ESPRESSO: a modular and open-source software project for quantum simulations of materials, *J. Phys.: Condens. Matter*, 2009, **21** 395502.
26 P. Giannozzi, O. Andreussi, T. Brumme, M. B. Nardelli, M. Calandra, R. Car, C. Cavazzoni, D. Ceresoli, M. Cococcioni, N. Colonna, I. Carnimeo, A. Dal Corso, S. de Gironzoli, P. Delugas, R. A. DiStasio Jr A. Ferretti, A. Floris, G. Fratesi, G. Fugallo, R. Gebauer, U. Gerstmann, F. Giustino, T. Gorni, J. Jia, M. Kawamura, H-Y. Ko, A, Kokalj, E. Küçükbenli, M. Lazzeri, M. Marsili, N. Marzari, F. Mauri, N. L. Nguyen, H-V; Nguyen, A. Otero-de-la-Roza, L. Paulatto, S. Poncé, D. Rocca, R. Sabatini, B. Santra, M. Schlipf, A. P. Seitsonen, A. Smogunov, I. Timrov, T. Thonhauser, P. Umari, N. Vast, X. Wu, S. Baroni, Advanced capabilities for materials modelling with Quantum ESPRESSO, *J. Phys.: Condens. Matter*, 2017, **29** 465901.